

TRAVELING WAVE SOLUTIONS OF FOURTH ORDER PDES FOR IMAGE PROCESSING

J. B. GREER ^{†§¶} AND A. L. BERTOZZI ^{‡§¶}

Key words. fourth order diffusion, image denoising, traveling waves, edge detection, Conley Index, advection diffusion, dynamical systems, nonlinear PDEs

Abstract. The authors introduce two nonlinear advection diffusion equations, each of which combines Burgers' convection with a fourth order nonlinear diffusion previously designed for image denoising. One equation uses the L^2 -curvature diminishing diffusion of You and Kaveh (IEEE Trans. Image Process., October 2000), and the other uses the 'Low Curvature Image Simplifiers' diffusion of Tumblin and Turk (SIGGRAPH, August 1999). The new PDEs are compared with a third advection diffusion equation that combines Burgers' convection with a second order diffusion recommended by Perona and Malik for denoising and edge detection (IEEE Trans. Pattern Anal. Machine Intell., July, 1990). We prove results regarding the existence and nonexistence of traveling wave solutions of each PDE. Visualizations of each ODE's phase space show qualitative differences between the two fourth order problems. The combined work gives insight into the existence of finite time singularities in solutions of the diffusion equations.

1. Introduction. We introduce two nonlinear advection diffusion equations that each combine Burgers' convection with a fourth order nonlinear diffusion intended for image processing:

$$u_t + \left(\frac{1}{2}u^2\right)_x = -(g(u_{xx})u_{xx})_{xx} \tag{YK}$$

and

$$u_t + \left(\frac{1}{2}u^2\right)_x = -(g(u_{xx})u_{xxx})_x, \tag{TT}$$

with $g(s) = \frac{1}{1+s^2}$. Very little is known about the fourth order diffusions, despite recent demonstrations of their effectiveness for image denoising [28, 32]. The combined advection-diffusion equations have the possibility of smooth traveling wave solutions approximating Burgers' shocks. We prove rigorously that such smooth traveling wave solutions of (YK) do not exist for sufficiently large jumps, whereas smooth traveling wave solutions of (TT) exist for all jump values. These results suggest very different behavior of the fourth order nonlinear imaging equations introduced by You and Kaveh [32] and Tumblin and Turk [28].

1.1. Nonlinear PDEs for image denoising. Nonlinear PDEs are now commonly used in image processing for issues ranging from edge detection, denoising, and image inpainting, to texture decomposition. Second order PDEs for image processing date back to the seminal works of Mumford-Shah [21], Rudin-Osher-Fatemi [25], and Perona-Malik [23]. All of these methods are based on a nonlinear version of the heat equation,

$$u_t = \nabla \cdot ((g(|\nabla u|)\nabla u), \tag{1.1}$$

[†]Department of Mathematics, Duke University, Durham, NC 27708 (jbg33@math.duke.edu)

[‡]Department of Mathematics and Physics, Duke University, Durham, NC 27708 (bertozzi@math.duke.edu)

[§]Department of Mathematics, UCLA, Los Angeles, CA 90095

[¶]This work is supported by ONR grant N000140110290, NSF grant DMS-0074049, and ARO grant DAAD19-02-1-0055.

May 6, 2003

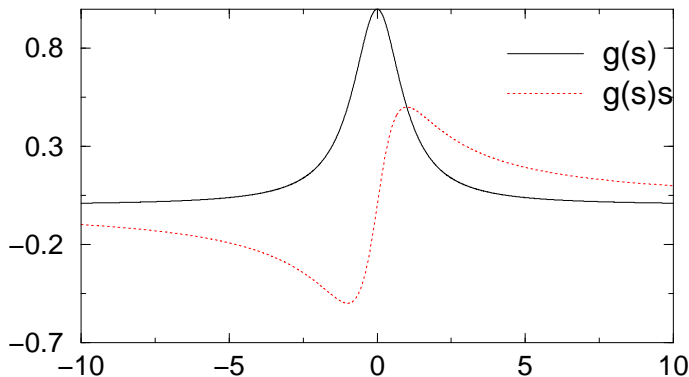


FIG. 1.1. An example thresholding function. $g(s)$ and $g(s)s$ are shown for $g(s) = \frac{1}{1+s^2}$.

in which the ‘thresholding function’ g is small in regions of sharp gradients. A number of mathematical issues arise with these equations and their use. For example, Perona-Malik suggest using a smooth, positive, and even function g that decays fast enough for large ∇u so that significant diffusion only takes place in regions away from image edges. Specifically, Perona and Malik required the existence of some $K > 0$ such that

$$\frac{d}{ds}(g(s)s) > 0 \text{ for } 0 < s < K, \quad (1.2)$$

and

$$\frac{d}{ds}(g(s)s) < 0 \text{ for } s > K. \quad (1.3)$$

However, the non-monotonicity of $g(s)s$ causes (1.1) to be ill-posed in regions of high gradients, and the ensuing dynamics result in a characteristic “staircase” instability. A typical thresholding function g is

$$g(s) = \frac{1}{k^2 + s^2}, \quad (1.4)$$

where k is a parameter used to establish a standard edge size for the image [11, 12, 15, 30, 31].

In the past few years, a number of authors have proposed analogous fourth order PDEs for edge detection and image denoising with the hope that these methods would perform better than their second order analogues [9, 10, 19, 20, 28, 29, 32]. Indeed there are good reasons to consider fourth order equations. First, fourth order linear diffusion damps oscillations at high frequencies (i.e. noise) much faster than second order diffusion. Second, there is the possibility of having schemes that include effects of curvature (i.e. the second derivatives of the image) in the dynamics, thus creating a richer set of functional behaviors. On the other hand, the theory of fourth order nonlinear PDEs is far less developed than that of their second order analogues. Also such equations often do not possess a maximum principle or comparison principle, and implementation of the equations could thus introduce artificial singularities or other undesirable behavior.

Some examples of fourth order equations include the L^2 -curvature gradient flow method of You and Kaveh [32],

$$u_t = -\Delta(g(\Delta u)\Delta u), \quad (1.5)$$

the Perona-Malik analogue by Wei [29],

$$u_t = -\nabla \cdot (g(\nabla u)\nabla\Delta u), \quad (1.6)$$

and Tumblin and Turk's 'Low Curvature Image Simplifiers' [28],

$$u_t + \nabla \cdot (g(D_{ij}u)\nabla\Delta u) = 0. \quad (1.7)$$

In (1.7), g is a function of the second derivatives of the image intensity function u . Although demonstrations of the application of these PDEs to images give similar results, it is unclear how the dynamics of these equations compare to each other. One immediate observation is that equation (1.5) is linearly ill-posed in regions of high curvature, while equation (1.7) is not.

A class of equations including (1.6) and (1.7) was studied in [14] by the authors, who proved global existence of H^1 solutions when the argument of g , in the form of derivatives of the intensity u , is convolved with a standard mollifier kernel. However, as is well known for some second order equations, as in (1.1), such mollification can turn an ill-posed problem into a well-posed problem [8]. The resulting numerical methods for the equations with mollification appear to smooth out, but not remove, undesirable artifacts of the method without mollification, such as the staircase instability of the Perona-Malik method.

1.2. The model equations. We introduce two model problems designed for studying the dynamics of these new image processing equations without mollification. Both are convection diffusion equations which can be studied by a combination of analytical and computational methods. We introduce a Burgers convection into the dynamics of the fourth order diffusions (1.5) and (1.7) in order to instigate shock or jump type behavior typical of edges in images. Such convective motion has real application in image processing. One area in particular is *image inpainting* [1, 2] in which image information is convectively flowed into a region where the image content is unknown. Thus our study gives insight into the behavior of hybrid imaging methods that combine diffusion and convection.

The two fourth order equations are compared with a second order convection diffusion equation that was introduced in [13] and [17]. This equation combines a Burgers convection term with the second order diffusion of (1.1). The authors of [13] and [17] share our motivation of using these equations as tools for understanding the diffusion dynamics.

The three model equations that we consider are

$$u_t + \left(\frac{1}{2}u^2\right)_x = (g(u_x)u_x)_x, \quad (PM)$$

$$u_t + \left(\frac{1}{2}u^2\right)_x = -(g(u_{xx})u_{xx})_{xx}, \quad (YK)$$

and

$$u_t + \left(\frac{1}{2}u^2\right)_x = -(g(u_{xxx})u_{xxx})_x. \quad (TT)$$

In each equation, we use the thresholding function

$$g(s) = \frac{1}{1+s^2}, \quad (1.8)$$

as in [23]. Many of our results can be easily generalized to thresholding functions g which satisfy the properties stated in [23]. Remarks are made regarding possible generalizations of our results.

We are interested in one overarching question for all three problems: when do the equations have smooth solutions, and when do they develop singularities (jumps in u or its derivatives)? This fundamental question arises when using such methods for image processing. Moreover, if a singularity forms, it is unclear whether a solution to the equation will continue to exist, perhaps as a weak or distribution solution, as is the case with shock dynamics.

We focus on a special class of similarity solutions – *traveling waves* of the form $u(x - ct)$. This traveling wave ansatz reduces the fourth order PDEs (YK) and (TT) to third order ODEs, to which we apply phase plane analysis from dynamical systems theory, as well as rigorous analysis using Conley index theory and estimates involving Lyapunov functions. Analyzing the simpler Perona-Malik equation (PM) is much more straightforward, however it gives some insight and provides a standard for comparison with the more complicated fourth order equations.

Our approach in this paper has been successfully used for other fourth order nonlinear equations that model physical systems. A mathematically similar family of PDEs are the lubrication equations used to model thin liquid films under the influence of surface tension. These equations take the form

$$u_t + \nabla \cdot (m(u)\nabla\Delta u) = 0,$$

where $m(u)$ is typically degenerate (i.e. f vanishes when u vanishes). Convection in thin films can arise due to body forces such as gravity or surface stresses involving gradients of surface tension. Recent analysis of traveling waves for the PDE

$$u_t + (f(u))_x = -(u^3 u_{xxx})_x$$

has led to an understanding of compressive and undercompressive shock dynamics in driven films [3, 4, 6, 7], and we consider some of the analytical methods for these problems in our study of traveling waves for image processing.

1.3. Organization. We derive traveling wave ODEs for all three PDEs in Section 2. By restricting to traveling wave solutions, the problems simplify to nonlinear ODEs. Sections 3 - 5 each contain an analysis of one of the three traveling wave ODEs. We first consider the simpler problem (PMODE) in Section 3 and use it as a standard for comparing (YKODE), discussed in Section 4, and (TTODE), considered in Section 5. The three sections share the same outline. We first prove analytic results for the considered ODE. These results are then illustrated with phase plane visualizations which also provide strong evidence for ODE properties that are not proved here. We close each section with a numerical demonstration of the PDE behavior and its relationship with the corresponding ODE.

2. Traveling wave solutions to PDEs. Traveling Waves are similarity solutions of the form

$$u(x, t) = \phi(x - ct), \tag{2.1}$$

where $c \in \mathbb{R}$ is the wave speed. By substituting (2.1) into the PDE, we reduce the problem to an ODE in the variable $\xi = x - ct$. ODEs are typically easier to study, as there are many well understood analytical and numerical methods for examining their qualitative behavior.

In this paper we consider traveling wave solutions that satisfy

$$\lim_{\xi \rightarrow -\infty} \phi(\xi) = u_L \text{ and } \lim_{\xi \rightarrow +\infty} \phi(\xi) = u_R. \quad (2.2)$$

Such solutions correspond to trajectories connecting $\phi = u_L$ to $\phi = u_R$ in the phase space of the traveling wave ODE. They give diffusive shocks, similar to those for the viscous Burgers equation [18]. The values of u_L and u_R determine the viscous shock's wave speed, c .

2.1. ODEs resulting from equations (PM), (YK), and (TT). Assume

$$u(x, t) = \phi(x - ct) = \phi(\xi), \quad (2.3)$$

for some real number c to be determined. Using the notation $\phi' := \frac{d}{d\xi}\phi$, and substituting (2.3) into equations (PM), (YK), and (TT), we derive the ODEs

$$\phi'(\phi - c) = (g(\phi')\phi')', \quad (2.4)$$

$$\phi'(\phi - c) = -(g(\phi'')\phi'')'' \quad (2.5)$$

and

$$\phi'(\phi - c) = -(g(\phi''')\phi''')' \quad (2.6)$$

respectively. Assuming (2.2) and that all of the derivatives of ϕ decay at infinity, integrating each ODE yields

$$r(\phi) = g(\phi')\phi', \quad (PMODE)$$

$$r(\phi) = -(g(\phi'')\phi'')' \quad (YKODE)$$

and

$$r(\phi) = -g(\phi''')\phi''', \quad (TTODE)$$

where

$$r(\phi) := \frac{1}{2}\phi^2 - c\phi + \frac{1}{2}u_L u_R, \quad (2.7)$$

with wave speed

$$c = \frac{1}{2}(u_L + u_R). \quad (2.8)$$

For reference, we call (PMODE) the Perona-Malik ODE, (YKODE) the You-Kaveh ODE, and (TTODE) the Tumblin-Turk ODE. Each ODE has two equilibrium points: L , where $\phi = u_L$, and R , where $\phi = u_R$. A trajectory of one of the given ODEs is a traveling wave solution of the respective PDE, if and only if that trajectory is a heteroclinic orbit connecting L and R . Each equation also has an entropy condition (which we derive) requiring $u_L > u_R$ for such an orbit to exist. This entropy condition is analogous to that of the viscous Burgers' equation [18].

2.2. Reducing the number of parameters. Consider (PMODE) for a given pair u_L and u_R , and corresponding wave speed, $c = \frac{1}{2}(u_L + u_R)$. Letting $\Phi = \phi - c$, equation (PMODE) becomes

$$\frac{1}{2} \left(\Phi^2 - \frac{1}{4}(u_R - u_L)^2 \right) = g(\Phi')\Phi'. \quad (2.9)$$

The dynamics of (PMODE) and (2.9) are affected solely by the difference between u_L and u_R . Changing their average, which gives the wave speed c , alters ϕ by only an added constant. The same holds true for (YKODE) and (TTODE).

For simplicity, we consider only the case $c = 0$, and we do so without loss of generality. All of our computational examples are done with $\phi(0) = c = 0$. These ODE solutions correspond to PDE solutions that travel with zero speed. We study the full range of behavior of the traveling wave ODEs by adjusting only one parameter, $\gamma := u_L > 0$. Insisting $c = 0$ forces $u_R = -\gamma$.

2.3. Comparing the traveling wave ODEs. In [17], Kurganov, Levy, and Rosenau proved the existence of traveling wave solutions of (PM) for the case $g(s) = \frac{1}{1+s^2}$. Traveling wave solutions exist for only a small range of left and right states. In particular, if u_L is much larger than u_R , the ODE will not have a solution connecting L to R . We generalize the results of [13] and [16] in Section 3, which contains a proof of the existence of solutions of (PMODE) for the general class of functions g satisfying the properties listed by Perona and Malik. By studying equations (PM) and (PMODE), we develop a framework for analyzing the higher order equations. In Section 3.4, we compare solutions of (PMODE) with the PDE (PM). Numerical experiments show a one-to-one correspondence between heteroclinic orbits of the ODE, and attracting steady state solutions of the PDE. When there is no trajectory connecting L to R in the ODE, a jump discontinuity forms in the PDE. We show that this restriction of left and right states stems from a singularity in the ODE which is caused by the lack of monotonicity of $g(s)$ s. The same dilemma also occurs in (YKODE), and we establish results in Section 3 that parallel the higher order problem.

The higher order diffusion makes analytical results more difficult to obtain for equations (YKODE) and (TTODE). However, in Section 4 we prove that equation (YKODE) does not have a smooth solution connecting L and R for large γ . By studying the ODE phase plane with the method introduced by [3], we discover that the unstable manifold of the left state intersects the stable manifold of the right state only when γ is small enough – just as in the second order case. We conclude the section by comparing the ODE solutions with the PDE (YK).

The Tumblin-Turk ODE is remarkably different from the other two ODEs. In Section 5, we use a topological argument to prove that equation (TTODE) has smooth solutions connecting L and R , for all $\gamma > 0$. Cross-sections of its phase plane illustrate the key differences between the phase plane geometries of (YKODE) and (TTODE). Once again, we follow the discussion with numerical computations of the PDE.

3. Perona-Malik with advection. Equation (PM) is carefully studied in [13] and [17]. We review and expand upon those results here, as they provide an excellent foundation for our analysis of equations (YK) and (TT). We first prove that (PMODE) has an orbit corresponding to a traveling wave solution of (PM) only when $\gamma > 0$ is smaller than a critical value, γ_c . This result is followed with a numerical and asymptotic description of solutions of (PMODE) for $\gamma > \gamma_c$.

3.1. The traveling wave ODE. We consider a general thresholding function g , as described in the introduction. Define

$$F(s) = g(s)s, \quad (3.1)$$

so that equation (PMODE) can be written as

$$r(\phi) = F(\phi').$$

Since $g(s)s$ is bounded, we can only define F^{-1} on a subset of \mathbb{R} . F^{-1} has three branches that depend on the unique K satisfying

$$g'(K)K + g(K) = 0. \quad (3.2)$$

Two of these branches correspond to the regions $|s| > K$ where $\frac{d}{ds}(g(s)s) < 0$. The third is an interior branch with its range centered around zero and corresponds to the interval $|s| < K$, where $\frac{d}{ds}(g(s)s) > 0$. We define F^{-1} on the interior branch, since our traveling waves have $\phi' \rightarrow 0$ as $\xi \rightarrow \pm\infty$. With this definition, we rewrite (PMODE) as

$$\phi' = F^{-1}(r(\phi)),$$

with the requirement

$$|r(\phi)| \leq F(K) = g(K)K. \quad (3.3)$$

This condition is satisfied if and only if

$$0 \leq \gamma \leq \sqrt{2g(K)K}, \quad (3.4)$$

and is essential to proving the following theorem, which is proved in [17] for the specific case $g(s) = \frac{1}{1+s^2}$.

THEOREM 1. *Let g be a smooth, positive, and non-increasing function of $|s|$, with some $K > 0$ satisfying*

$$\frac{d}{ds}(g(s)s) > 0 \text{ for } |s| < K, \text{ and } \frac{d}{ds}(g(s)s) < 0 \text{ for } |s| > K.$$

Then the ODE (PMODE) has a continuous solution $\phi(\xi)$ satisfying

$$\lim_{x \rightarrow -\infty} \phi(\xi) = \gamma \text{ and } \lim_{x \rightarrow +\infty} \phi(\xi) = -\gamma, \quad (3.5)$$

if and only if

$$0 \leq \gamma \leq \sqrt{2g(K)K}. \quad (3.6)$$

Proof. Any traveling wave solution of (PM) satisfying (2.2) corresponds to a trajectory of (PMODE) connecting L , the point $\phi = \gamma$, to R , the point $\phi = -\gamma$. Such a trajectory can only exist when $\gamma > 0$, since $F^{-1}(r(\phi)) < 0$ for $|\phi| < |\gamma|$. This is analogous to the Lax-Oleinik entropy condition for Burgers' Equation [18]. If $\gamma \leq 1$, $r(\phi) \leq \sqrt{2g(K)K}$ for all $\phi \in (-\gamma, \gamma)$, so the existence of an orbit connecting L to R is obvious.

Smooth Solutions of Equation (PMODE)

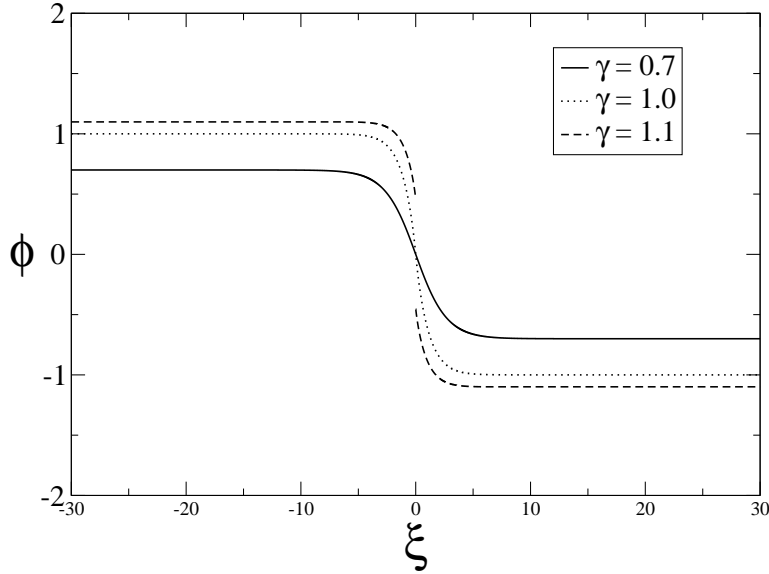


FIG. 3.1. **Heteroclinic orbits of (PMODE) for different values of γ .** Solutions connecting L to R only exist for $\gamma \leq 1$. For $\gamma = 1.1$, we show two trajectories – one starting near L , and one approaching R .

Suppose $\gamma > \sqrt{2g(K)K}$. Any continuous heteroclinic orbit, ϕ , connecting L to R must have $\phi(\xi_0) = 0$ for some ξ_0 . We calculate $|r(0)| = \frac{1}{2}\gamma^2 > g(K)K$ and remember that $g(s)s \leq g(K)K$ for all s , implying that ϕ can not possibly satisfy (PMODE). \square

Remark. For the remainder of the paper, we restrict the main part of our discussion to $g(s) = \frac{1}{1+s^2}$, for which $K = 1$, and $|g(s)s| \leq \frac{1}{2}$. Comments regarding generalizing our results to other thresholding functions will be made throughout the paper.

Figure 3.1 shows solutions of (PMODE) for $g(s) = \frac{1}{1+s^2}$ and various values of γ . Equation (PMODE) has a trajectory connecting L to R only when $\gamma \leq 1$. When $\gamma > 1$, (PMODE) only has a solution near the equilibrium points. Starting with ϕ slightly smaller than γ , we integrate forward in time until $|r(\phi)| = \frac{1}{2} = \max\{g(s)s\}$. We then start with ϕ slightly larger than $-\gamma$, and integrate backward in time until $|r(\phi)| = \frac{1}{2}$. Figure 3.1 shows $\phi(\xi)$ for $\gamma = 1.1$ in the regions of ξ where $F^{-1}(r(\phi(\xi)))$ is defined.

3.2. Second order version of (PMODE). Expanding the right side of (2.4) yields a second order form of the traveling wave ODE for (PM):

$$\phi' = ((g'(\phi')\phi' + g(\phi'))\phi''). \quad (3.7)$$

Unlike (PMODE), equation (3.7) does not depend on the choice of γ . Due to the properties of g , equation (3.7) becomes singular as $|\phi'| \rightarrow 1$. We rewrite (3.7) as a

Phase Plane Portrait

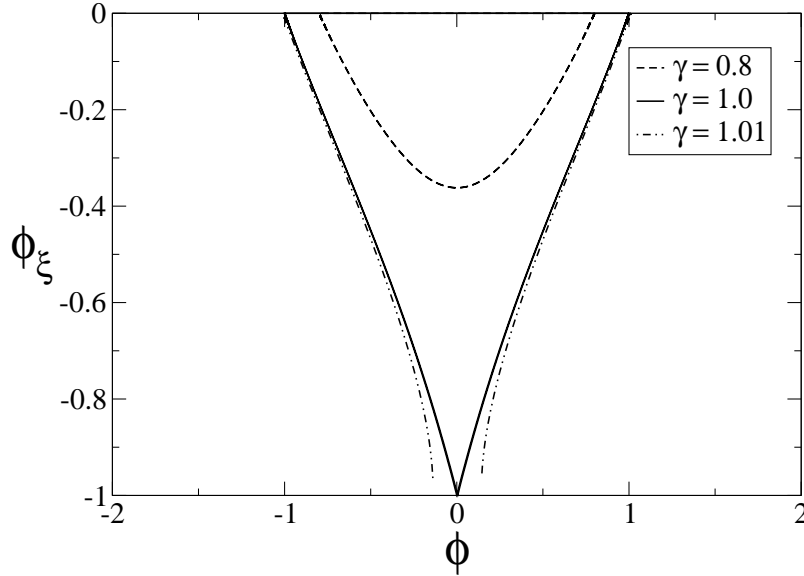


FIG. 3.2. **Phase plane of ODE system (3.8).** A series of trajectories are plotted for different values of γ . If $\gamma > 1$, any connection from $(\gamma, 0)$ to $(-\gamma, 0)$ would need to pass through the line of singularity, $\phi' = -1$.

system of two ODEs:

$$\phi' = v, \quad v' = \frac{\phi v}{g'(v)v + g(v)}. \quad (3.8)$$

System (3.8) has a line of equilibrium points at $v = 0$. Figure 3.2 shows integral curves where $\phi \rightarrow -\gamma$ as $\xi \rightarrow \infty$ and $\phi \rightarrow \gamma$ as $\xi \rightarrow -\infty$. Each integral curve coincides with a particular value of γ . As γ increases, the integral curves move toward the singular line $v = -1$, clearly illustrating the results of Section 3, and showing why heteroclinic orbits of (PMODE) do not exist for large γ . Such traveling waves would require ϕ' to pass through the singular value $\phi' = -1$.

3.3. Singularities in solutions of (PMODE). We now consider the behavior of singular solutions of (PMODE). We examine two cases: $\gamma > 1$ and $\gamma = 1$. When $\gamma > 1$, there is no traveling wave solution. We consider a trajectory $\phi(\xi)$ starting near L and moving toward R , and examine ξ_0 satisfying

$$\lim_{\xi \rightarrow \xi_0^-} \phi'(\xi) = -1 \quad \text{and} \quad \lim_{\xi \rightarrow \xi_0^-} \phi(\xi) = \phi^*,$$

for some $\phi^* > 0$. We have $\phi' \phi \rightarrow -\phi^*$ as $\xi \rightarrow \xi_0$. Near $\phi' = -1$,

$$g'(\phi')\phi' + g(\phi') \sim \frac{1}{2}(\phi' + 1),$$

so

$$\int_{\xi}^{\xi_0} -\phi^* \sim \int_{\xi}^{\xi_0} (\phi' + 1)\phi'',$$

and

$$\phi'(\xi) \sim \sqrt{4\phi^*(\xi_0 - \xi)} - 1. \quad (3.9)$$

When $\gamma = 1$, there is a non-smooth traveling wave solution. In this case, $\phi^* = 0$ and $\phi(\xi) \sim -(\xi_0 - \xi)$ near $\xi = \xi_0$, so

$$\phi'(\xi) \sim \sqrt{2}|\xi - \xi_0| - 1. \quad (3.10)$$

This singular behavior is demonstrated by the solid line trajectory in Figure 3.2.

3.4. Second order PDE computations. We test the stability of each traveling wave solution found from (PMODE) by choosing an initial condition near the traveling wave and numerically integrating the PDE (PM). We use a fully implicit scheme with an adaptive time step, and use Newton's method to approximate solutions of the nonlinear system.

Figure 3.3 shows computations for $\gamma = 1$ and $\gamma = 1.1$. When $0 \leq \gamma \leq 1$, equation (PMODE) has a heteroclinic orbit between L and R . The case $\gamma = 1$ is discussed in Section 3.3. This traveling wave, ϕ , is continuous, but non-smooth. ϕ' behaves like (3.10) near $\phi = 0$. Given an initial condition near this traveling wave, the PDE solution converges to the traveling wave solution, as long as the gradient of the initial condition is not too large (for large gradients, (PM) becomes ill-posed, and a jump discontinuity occurs). There is no traveling wave solution for $\gamma > 1$, as seen in the computations for $\gamma = 1.1$; although the initial condition is smooth with small gradient, a discontinuity develops in finite time, and the long time solution has a jump discontinuity.

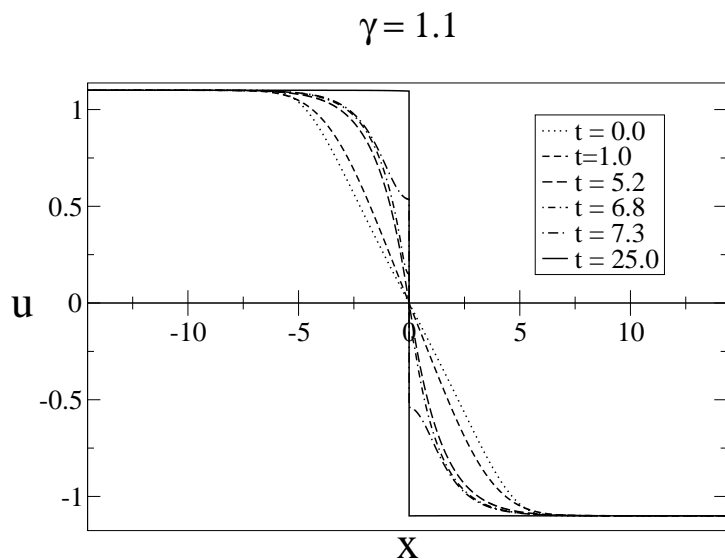
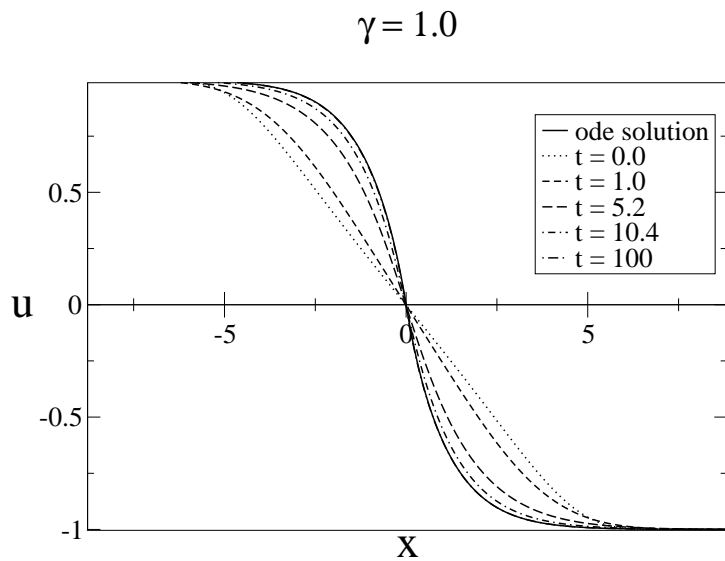


FIG. 3.3. PDE (PM) solution, u , for $\gamma = 1.0$ and $\gamma = 1.1$. When $\gamma = 1.0$, u approaches the corresponding traveling wave ODE solution as t increases. $\gamma = 1.0$ is the maximum value for which the PDE has a traveling wave connecting γ to $-\gamma$. When $\gamma = 1.1$, u forms a jump discontinuity in finite time.

4. You-Kaveh with advection. Equation (YK) shares many of the properties of (PM). We prove that orbits of (YKODE) corresponding to traveling wave solutions of (YK) do not exist when γ is too large. This nonexistence follows from a singularity in (YKODE) that is analogous to that of (PMODE). We study the phase space of (YKODE) for evidence of the existence of traveling wave solutions when γ is small. For simplicity, we assume $g(s) = \frac{1}{1+s^2}$, which is the thresholding function chosen by You and Kaveh in [32]. However, our results generalize to other thresholding functions as described in Section 1.1.

4.1. The traveling wave ODE. Equation (YKODE) can be expanded to

$$r(\phi) = -(g'(\phi'')\phi'' + g(\phi''))\phi'''. \quad (4.1)$$

Since $g'(s)s + g(s) = 0$ for $s = \pm 1$, we immediately see a similarity to (PMODE): a solution ϕ of (YKODE) becomes singular in ϕ''' when $|\phi''| \rightarrow \pm 1$, just as a solution ϕ of (PMODE) becomes singular in ϕ'' when $|\phi'| \rightarrow \pm 1$.

Remark. For general functions g as described in [23], there exists a $K > 0$ satisfying (3.2), so equation (4.1) is singular at $\phi'' = \pm K$. A solution ϕ of (PMODE) becomes singular in ϕ'' when $|\phi'| \rightarrow K$, and a solution ϕ of (YKODE) becomes singular in ϕ''' when $|\phi''| \rightarrow K$.

4.2. Lyapunov function for the You-Kaveh ODE. Equation (YKODE) has a Lyapunov function. Multiplying (YKODE) by ϕ' and integrating, we have

$$\int_{-\infty}^{\xi} r(\phi(y))\phi'(y)dy + g(\phi''(\xi))\phi'(\xi)\phi''(\xi) = \int_{-\infty}^{\xi} g(\phi''(y))(\phi''(y))^2 dy. \quad (4.2)$$

Define

$$\mathcal{R}(s) = \int^s r(\alpha)d\alpha.$$

We see that

$$\mathcal{L}_1(\xi) = \mathcal{R}(\phi(\xi)) + g(\phi''(\xi))\phi'(\xi)\phi''(\xi) \quad (4.3)$$

is nondecreasing, since

$$\frac{d}{d\xi}\mathcal{L}_1(\xi) = g(\phi''(\xi))(\phi''(\xi))^2 \geq 0. \quad (4.4)$$

This Lyapunov function establishes the entropy condition, $\gamma > 0$. Also, since $\mathcal{L}_1(\xi) = \mathcal{R}(\phi(\xi))$ at extrema of ϕ , the structure of \mathcal{R} implies a uniform bound on all bounded solutions of (YKODE). Figure 4.1 shows \mathcal{R} for a particular γ . \mathcal{R} 's essential behavior remains the same for different values of $\gamma > 0$. \mathcal{R} is a cubic polynomial with a local maximum at γ , and a local minimum at $-\gamma$. $\mathcal{R}(\phi)$ strictly increases for $\phi < -\gamma$ and for $\phi > \gamma$, while it strictly decreases for $-\gamma < \phi < \gamma$. Let

$$\bar{\phi} = 2\gamma \quad \text{and} \quad \underline{\phi} = -2\gamma. \quad (4.5)$$

$\mathcal{R}(\phi)$ for $\gamma = 2$

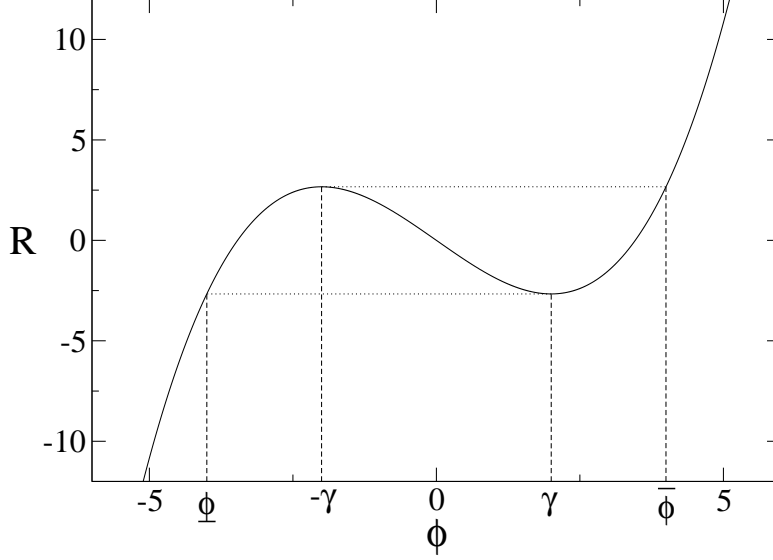


FIG. 4.1. $\mathcal{R}(\phi)$ for $\gamma = 2$. We mark the maximum and minimum values, $\bar{\phi}$ and $\underline{\phi}$, for a bounded solution of (YKODE).

A simple calculation shows

$$\mathcal{R}(\bar{\phi}) = \mathcal{R}(-\gamma) \quad \text{and} \quad \mathcal{R}(\underline{\phi}) = \mathcal{R}(\gamma). \quad (4.6)$$

We now prove that $\bar{\phi}$ and $\underline{\phi}$ are respectively upper and lower bounds on the set of all bounded solutions of (YKODE).

LEMMA 4.1. *Let $\bar{\phi}$ and $\underline{\phi}$ be defined by (4.5). Any bounded solution ϕ of (YKODE) must satisfy*

$$\underline{\phi} \leq \phi(\xi) \leq \bar{\phi} \quad (4.7)$$

for all $\xi \in \mathbb{R}$.

Proof. Consider any bounded solution ϕ of (YKODE). There exists a ξ_0 such that $\underline{\phi} < \phi(\xi_0) < \bar{\phi}$. Otherwise $r(\phi(\xi))$ would be bounded away from zero for all ξ , thus bounding $g(\phi'')\phi'''$ away from zero and causing ϕ to become unbounded. Suppose there exists a ξ_1 with $\phi(\xi_1) > \bar{\phi}$. Then ϕ has a local extremum, $\phi(\xi_M) = \phi_M > \bar{\phi}$, otherwise $r(\phi)$ would remain bounded away from zero, implying that ϕ is unbounded. Since $\phi' = 0$ at extrema,

$$\mathcal{L}_1(\phi(\xi_M)) = \mathcal{R}(\phi(\xi_M)) > \mathcal{R}(-\gamma) > \mathcal{R}(\gamma).$$

Consider $\phi(\xi)$ for $\xi > \xi_M$. If $\phi > \bar{\phi}$ for all $\xi > \xi_M$, then ϕ''' is strictly bounded away from zero for all $\xi > \xi_M$, thus implying that ϕ is unbounded. So ϕ must either have a local extrema $\phi_* < \bar{\phi}$, or approach a constant value of γ or $-\gamma$ as $\xi \rightarrow \infty$. In the first case, $\mathcal{R}(\phi_*) < \mathcal{R}(\phi_M)$, a contradiction. In the second, $\phi'(\xi) \rightarrow 0$ and either

$L(\xi) \rightarrow \mathcal{R}(\gamma)$ or $L \rightarrow \mathcal{R}(-\gamma)$, as $\xi \rightarrow \infty$. Both possibilities contradict the fact that L increases monotonically. Similarly arguing how $\phi(\xi)$ must behave as $\xi \rightarrow -\infty$ shows that $\phi \geq \underline{\phi}$. \square

As already noted, $|\phi''| = 1$ is a singular value for (YKODE). We use the Lyapunov function to prove the following lemma, which shows that smooth heteroclinic orbits are forbidden from crossing this value. Lemma 4.2 is essential for showing that (YKODE) does not have a smooth heteroclinic orbit connecting L to R when γ is too large.

LEMMA 4.2. *Let $\phi(\xi)$ be a smooth heteroclinic orbit connecting L to R . Then $\forall \xi$, $|\phi''(\xi)| \leq 1$.*

Proof. We show $\phi''(\xi) \leq 1$. Proving $\phi''(\xi) \geq -1$ follows the same line of argument. Suppose that ϕ is a smooth trajectory for which there exists a ξ such that $\phi''(\xi) > 1$. We show that ϕ can not connect L to R . Our argument follows directly from the ODE and its Lyapunov function. Our assumptions on ϕ imply the existence of a ξ_c and an $\epsilon > 0$ such that $\phi''(\xi_c) = 1$, $\phi''(\xi) < 1$ for $\xi \in (\xi_c - \epsilon, \xi_c)$, and $\phi''(\xi) > 1$ for $\xi \in (\xi_c, \xi_c + \epsilon)$. Since ϕ is smooth, and $g'(1) + g(1) = 0$, we must have $r(\phi(\xi_c)) = 0$, and therefore $\phi(\xi_c) = \pm\gamma$. Suppose $\phi(\xi_c) = \gamma$. Then the ODE implies $\phi'(\xi_c) > 0$. Also $\phi'''(\xi) > 0$ for $\xi \in (\xi_c, \xi_c + \epsilon)$, and since both $\phi'(\xi)$ and $\phi''(\xi)$ are positive on the same interval, ϕ will continue to grow without bound, prohibiting it from being a heteroclinic orbit.

Now suppose $\phi(\xi_c) = -\gamma$ and that $\phi'''(\xi_c)$ is bounded. Then $\phi'(\xi_c) < 0$. Since $\phi < -\gamma$ and $\phi'' > 1$, $\phi'''(\xi) > 0$ for some interval of $\xi > \xi_c$, and ϕ'' will continue to increase until ϕ' becomes positive and ϕ once again intersects $-\gamma$. So there is some $\xi_* > \xi_c$ with $\phi(\xi_*) = -\gamma$, $\phi'(\xi_*) > 0$, and $\phi''(\xi_*) > 1$. So $\mathcal{L}_1(\xi_*) > \mathcal{R}(-\gamma)$, and ϕ can not be a heteroclinic orbit connecting L to R . \square

4.3. Nonexistence of traveling waves for Equation (YKODE). Integrating (YKODE) on an arbitrary interval $[\xi_1, \xi_2]$, we see

$$g(\phi''(\xi_2))\phi''(\xi_2) - g(\phi''(\xi_1))\phi''(\xi_1) = \int_{\xi_1}^{\xi_2} r(\phi(y))dy. \quad (4.8)$$

Since $|g(s)s| \leq \frac{1}{2}$, smooth solutions of (YKODE) are restricted by

$$\left| \int_{\xi_1}^{\xi_2} r(\phi(y))dy \right| \leq 1 \quad (4.9)$$

on any interval $[\xi_1, \xi_2]$. We now use (4.9) to show that when γ is too large, the You-Kaveh ODE does not have a smooth heteroclinic orbit between L and R .

THEOREM 4.3. *There exists a finite $C > 0$ such that (YKODE) has no smooth solution satisfying*

$$\lim_{\xi \rightarrow -\infty} \phi(\xi) = \gamma \text{ and } \lim_{\xi \rightarrow +\infty} \phi(\xi) = -\gamma \quad (4.10)$$

when $\gamma > C$.

Proof. Suppose ϕ is a smooth solution of (YKODE) that satisfies (4.10). Then ϕ must be a heteroclinic orbit connecting L to R , and there exists at least one ξ with $\phi(\xi) = 0$. Let ξ_0 be the minimum of all points ξ satisfying $\phi(\xi) = 0$. Let ξ_-

be the largest number satisfying both $\xi_- < \xi_0$ and $\phi(\xi_-) = \gamma$. Since $\phi''' > 0$ when $-\gamma < \phi < \gamma$, $\phi'(\xi) \leq 0$ for all $\xi \in [\xi_-, \xi_0]$. Otherwise both ϕ' and ϕ'' would become positive in (ξ_-, ξ_0) . ϕ' would have to become negative again so that $\phi(\xi_0) = 0$, but this would require that ϕ become larger than γ , contradicting the assumptions on ξ_- .

Let μ denote the minimum of ϕ' on $[\xi_-, \xi_c]$. Then restriction (4.9) implies

$$\begin{aligned} 1 &\geq \int_{\xi_-}^{\xi_c} -r(\phi(s)) ds = \int_{\xi_-}^{\xi_c} -r(\phi(s)) \frac{\phi'(s)}{\phi'(s)} ds \geq \frac{1}{\mu} \int_{\xi_-}^{\xi_c} -r(\phi(s)) \phi'(s) ds \\ &= \frac{1}{\mu} (\mathcal{R}(\gamma) - \mathcal{R}(0)). \end{aligned}$$

Since $\mu < 0$ and $\mathcal{R}(\gamma) < \mathcal{R}(0)$, the above gives

$$\mathcal{R}(0) - \mathcal{R}(\gamma) \leq |\mu|. \quad (4.11)$$

From the bounds on ϕ and ϕ'' given by Lemmas 4.1 and 4.2, we see that

$$|\mu| \leq 2\sqrt{2\gamma} \quad (4.12)$$

as a result of the following interpolation lemma.

LEMMA 4.4. *Suppose $f \in C^2(\mathbb{R})$ satisfies $|f| \leq M$ and $|f''| \leq C$. Then*

$$|f'| \leq 2\sqrt{CM}.$$

Proof. Given $x \in \mathbb{R}$, Taylor's theorem shows

$$f'(x) = \frac{f(x+2h) - f(x)}{2h} - f''(\xi)h \quad (4.13)$$

for all $h > 0$ and some $\xi \in [-h, h]$. The bounds on f and f'' give us

$$|f'(x)| \leq \frac{M}{h} + Ch.$$

Choosing $h = \sqrt{\frac{M}{C}}$ gives

$$|f'(x)|^2 \leq \left(\frac{M}{h} + Ch \right)^2 = 4MC.$$

□

Calculating

$$\mathcal{R}(0) - \mathcal{R}(\gamma) = \frac{1}{3}(\gamma)^3,$$

and combining (4.11) with (4.12) proves Theorem 4.3. □

Remark. Theorem 4.3 does not depend on the choice $g = \frac{1}{1+s^2}$. It only relies on the properties of thresholding functions as explained in [23] and in Section 1.1. In particular, the nonexistence follows mainly from the non-monotonicity of $g(s)s$.

4.4. The (YKODE) phase space. We rewrite (4.1) as a system of first-order ODEs:

$$\phi' = v, \quad v' = w, \quad w' = -\frac{r(\phi)}{g'(w)w + g(w)}. \quad (4.14)$$

System (4.14) has two equilibrium points, $L = (\gamma, 0, 0)$ and $R = (-\gamma, 0, 0)$. A traveling wave solution of (YK) satisfying (2.2) corresponds to a heteroclinic orbit connecting L to R . Let $W^s(L)$ and $W^u(L)$ denote respectively the stable and unstable manifolds of L , and define $W^s(R)$ and $W^u(R)$ in the same way.

Since $\gamma > 0$, $W^u(L)$ and $W^s(R)$ are both two-dimensional with complex eigenvalues, while $W^u(R)$ and $W^s(L)$ are one-dimensional manifolds. We follow the method used in [3] and [7]. We illustrate the unstable manifold of L by considering a set of initial values near L and integrating (4.14) forward in time. Each trajectory will approach $W^u(L)$. To visualize the manifold, we mark the intersections of each computed trajectory with a two-dimensional plane (a Poincaré section) in the phase space. This plane is chosen so that all trajectories intersect the plane transversely. Any two-dimensional manifold intersects the plane on a curve and any one-dimensional manifold intersects at a point. Picking initial points near R , and integrating the ODE backward in time produces trajectories approaching $W^s(R)$. Traveling wave solutions of (4.14) correspond to intersections of $W^u(L)$ with $W^s(R)$.

In each figure, initial values are taken at a distance of 10^{-7} to 10^{-5} from the corresponding equilibrium point. We consider the plane $\phi = 0$, denoted by Σ_0 . Any intersection of $W^u(L)$ with $W^s(R)$ must appear on Σ_0 . The symmetry of (4.14) implies that the restriction of $W^u(L) \cap W^s(R)$ to Σ_0 occurs on the line $w = 0$.

Figure 4.2 shows the intersection of stable and unstable manifolds of u_L and u_R with Σ_0 for $\gamma = 0.5$. Since $W^u(L)$ and $W^s(R)$ intersect each other, there is a heteroclinic orbit connecting L to R . One end of $W^u(L)$ spirals around the one-dimensional manifold, $W^u(R)$. Symmetry gives the same relationship between $W^s(R)$ and $W^s(L)$. As γ is increased, the spiral structure of $W^u(L)$ shifts toward the line $w = 1$, while $W^s(R)$ shifts toward $w = -1$. Figure 4.3 demonstrates that the manifolds do not have this spiral structure on Σ_0 when γ is too large. The one-dimensional manifolds $W^s(L)$ and $W^s(R)$ no longer intersect Σ_0 when these spiral structures disappear. Further increasing γ moves $W^u(L)$ and $W^s(R)$ way from each other. For large enough γ , $W^u(L)$ and $W^s(R)$ do not intersect each other, as seen in Figure 4.3, where $\gamma = 1.3$.

In Figure 4.4, we draw $W^u(L)$ for a sequence of γ values. $W^s(R)$ is not shown, since it can be deduced by reflecting $W^u(L)$ across the line $w = 0$. The two manifolds intersect only when the restriction of $W^u(L)$ to Σ_0 intersects the line $w = 0$. $W^u(L)$ (and consequently $W^s(R)$) shifts away from the line $w = 0$ as γ increases. For large enough γ , $W^u(L)$ does not intersect the line $w = 0$ at Σ_0 . As proved in Theorem 4.3, there is a value γ_c such that $W^u(L)$ and $W^s(L)$ do not intersect when $\gamma > \gamma_c$. Our numerical experiments suggest that $1.16 < \gamma_c < 1.17$.

4.5. Manifold boundaries caused by singularities in solutions of (YKODE).

$W^u(L)$ and $W^s(R)$ have boundaries caused by the ODE's singularity. Consider $\gamma = 1.0$, for which $W^u(L) \cap \Sigma_0$ is bounded above by $w = 1$. Certainly the manifold can not extend past $w = 1$, since (4.14) is singular there, but there is also a boundary on the opposite end of $W^u(L) \cap \Sigma_0$. This boundary is far from either line of singularity, $w = \pm 1$. Figure 4.5 shows the second derivative of trajectories near these top and bottom boundaries of $W^u(L) \cap \Sigma_0$. Let ξ_0 denote the value of ξ for

Intersections of Stable and Unstable Manifolds With Σ_0

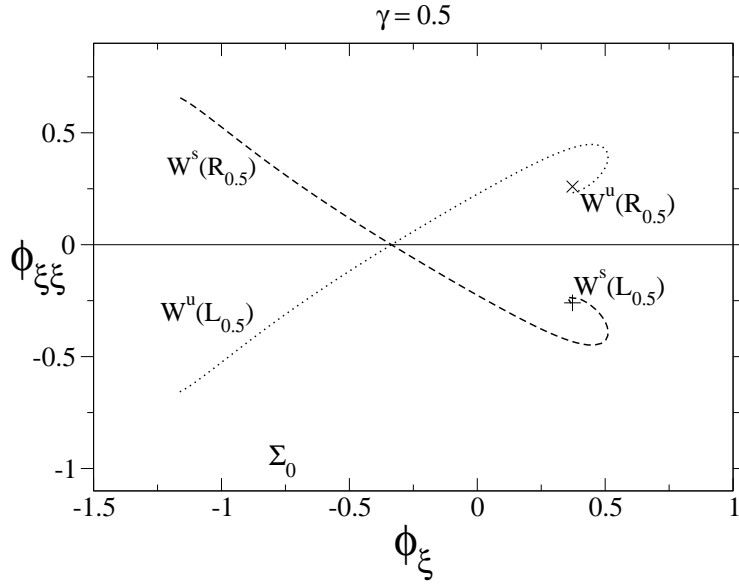


FIG. 4.2. **Cross-section of the phase plane of equation (YKODE) with $\gamma = 0.5$.** We show the intersections of the stable and unstable manifolds of both equilibrium points with the plane $\phi = 0$ (denoted Σ_0).

Intersections of $W^s(R_\gamma)$ and $W^u(L_\gamma)$ With Σ_0

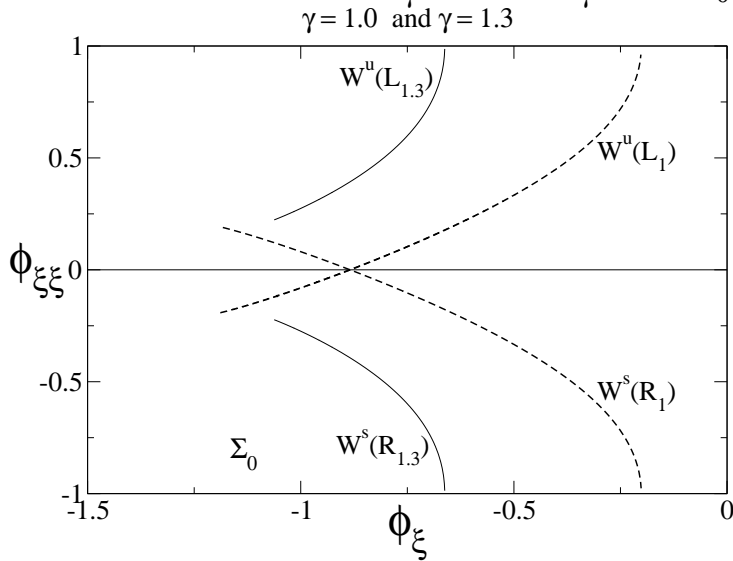


FIG. 4.3. **Changing manifolds of equation (YKODE) with increasing γ .** The intersections of $W^u(L)$ and $W^s(R)$ with Σ_0 are shown for $\gamma = 1.0$ and $\gamma = 1.3$. In both cases, $W^s(L)$ and $W^u(R)$ do not intersect Σ_0 . When $\gamma = 1.3$, $W^u(L)$ does not intersect $W^s(R)$, so there can be no traveling wave solution of the PDE.

Intersections of $W^u(L)$ with Σ_0

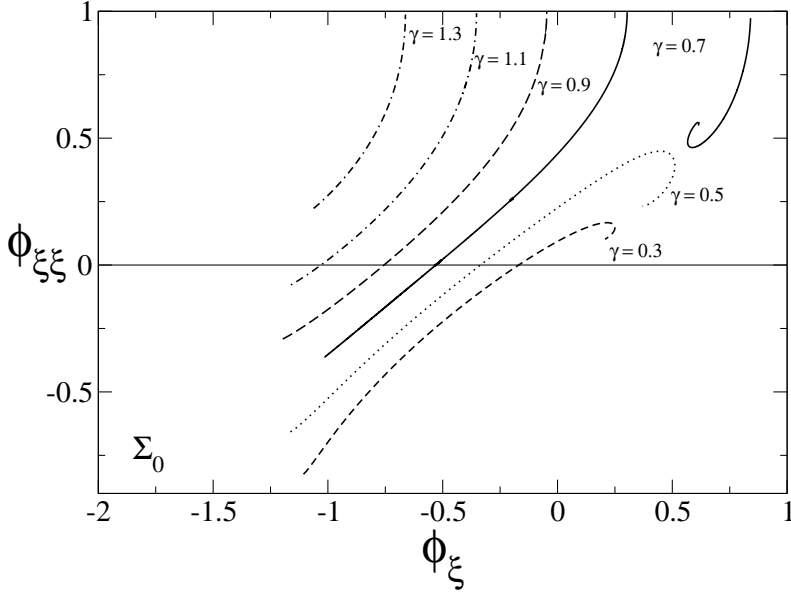


FIG. 4.4. $W^u(L) \cap \Sigma_0$ for equation (YKODE) with different values of γ . A traveling wave solution exists when $W^u(L) \cap \Sigma_0$ intersects the line $\phi'' = 0$. We see that no such intersection exists for large enough γ .

which a given trajectory $\phi(\xi)$ intersects Σ_0 (ξ_0 could be different for each trajectory). Near the top boundary, $\phi''(\xi_0)$ gets arbitrarily close to $\phi''(\xi_0) = -1$. Trajectories near the bottom boundary approach $\phi''(\xi_c) = -1$, for some $\xi_c < \xi_0$. We see that $\phi(\xi_c) \rightarrow \gamma$, since $\phi'''(\xi_c) \rightarrow 0$.

The singularities of solutions to (YKODE) are similar to those of (PMODE), but they occur in higher derivatives. Consider a trajectory ϕ with second derivative approaching -1 (the case $\phi'' \rightarrow 1$ is very similar). Assume there is some ξ_* with

$$\lim_{\xi \rightarrow \xi_*} \phi''(\xi) = -1 \text{ and } \lim_{\xi \rightarrow \xi_*} \phi(\xi) = \phi^*.$$

Again we have multiple cases, but this time they depend on the zeros of $r(\phi)$.

Case 1: $r(\phi^*) \neq 0$. This corresponds to the case $\gamma > 1$ for (PMODE). But now the singularity occurs in ϕ''' as $\xi \rightarrow \xi_*$.

$$\phi''(\xi) \sim 2\sqrt{r(\phi^*)(\xi_* - \xi)} - 1. \quad (4.15)$$

This singularity is demonstrated by trajectory near the top boundary of $W^u(L)$, drawn in Figure 4.5.

Case 2: $r(\phi^*) = 0$. Either $\phi^* = \gamma$ or $\phi^* = -\gamma$. It is easy to check that

$$\phi''(\xi) \sim \sqrt{2}|\xi - \xi_*| - 1. \quad (4.16)$$

Case 2 is demonstrated by the trajectory near the bottom boundary of $W^u(L)$, as seen in Figure 4.5. It also corresponds to a critical case for traveling wave solutions of (YKODE). We expect that there is some γ_c for which (YKODE) has a non-smooth traveling wave solution analogous to the solution of (PMODE) for $\gamma = 1$.

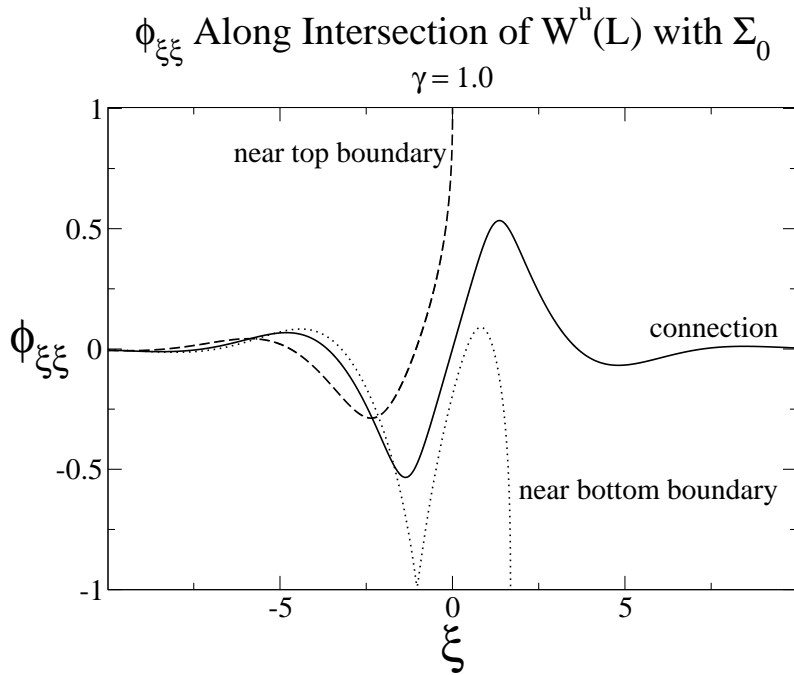


FIG. 4.5. **Trajectories of (YKODE) near the boundaries of $W^u(L)$ for $\gamma = 1.0$.** Shows the second derivatives of trajectories that pass near the top and bottom boundaries of $W^u(L) \cap \Sigma_0$. Trajectories near the top boundary have second derivatives approaching the singular value $w = 1$ as ϕ approaches 0, as can be seen from the phase portrait. Trajectories near the bottom boundary have a second derivative near $\phi'' = -1$, but not where $\phi = 0$. The traveling wave solution's second derivative is shown for comparison.

You-Kaveh Traveling Waves

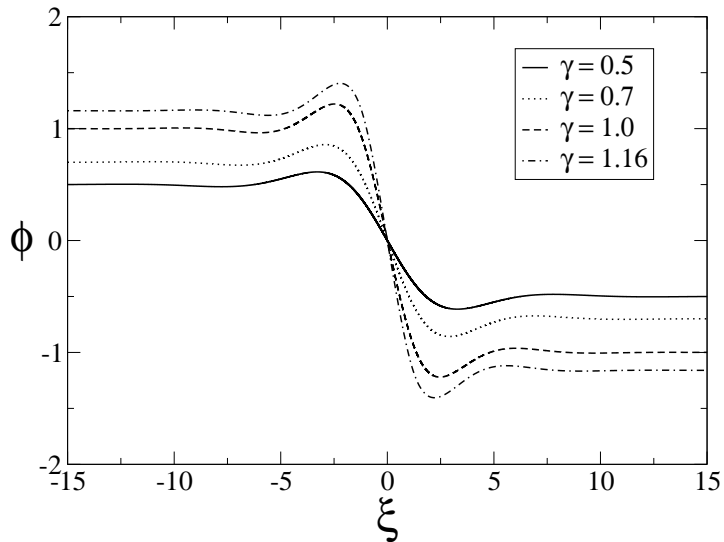


FIG. 4.6. **Traveling wave solutions of equation (YK).** Shown for different values of γ .

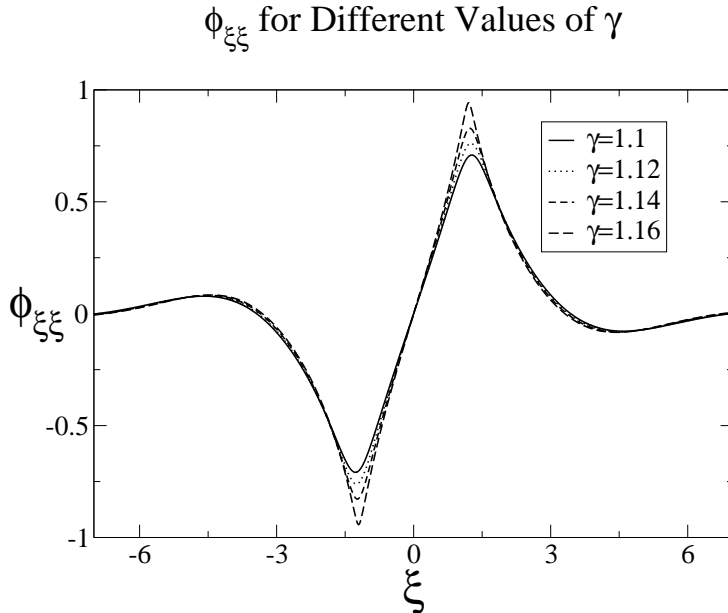


FIG. 4.7. The second derivatives of traveling wave solutions of equation (YK). Traveling waves for γ near 1.16 have second derivatives near the singular value $w = -1$.

4.6. Traveling wave solutions of equation (YK). Solutions of ODE (4.1) that correspond to traveling waves connecting L to R are given by the intersection of $W^u(L)$ with $W^s(R)$. Our study of the phase space shows that there is at most one such intersection for any given γ . The traveling waves shown in Figure 4.6 were produced by finding this intersection.

In Figure 4.7, we provide graphs of the second derivative of traveling wave solutions. In each case, $|\phi''|$ is bounded by 1 as expected. The local extrema of ϕ'' are achieved at $\phi = \pm\gamma$, where $\phi''' = 0$. As γ increases, these extreme values approach the singular values $\phi'' = \pm 1$. Because of the ODE's symmetry, ϕ'' approaches a singular value in two places. ϕ'' approaches -1 when $\phi = \gamma$, and it approaches +1 when $\phi = -\gamma$.

To show that these traveling waves are stable, we implement equation (YK) with a fully implicit scheme and adaptive time step. The correspondence between (YK) and (YKODE) is not as clear as it is for (PM) and (PMODE). The numerics become very difficult for γ near the range of nonexistence of traveling waves. In this parameter range, the PDE numerics do not converge nicely to a traveling wave solution, even when our ODE numerics suggests one exists. It is not clear whether this difficulty results from the numerics or from the PDE. We show an example with a smaller γ in Figure 4.8. In this case, the PDE solution clearly converges to the solution of (YKODE).

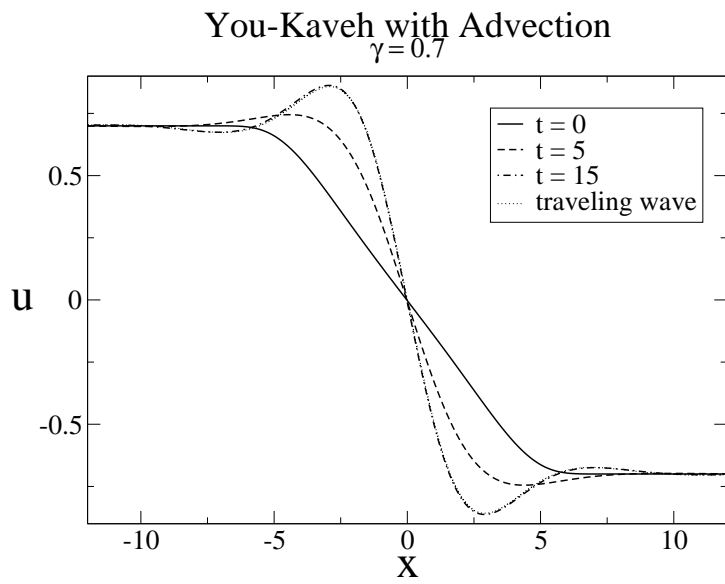


FIG. 4.8. Approximate solution of (YK). When $\gamma = 0.7$, u approaches the traveling wave solution given by (YKODE).

5. Tumblin-Turk with advection. We show that (TT) is qualitatively different from both (PM) and (YK). We first use a topological argument to prove that for all $\gamma > 0$, (TTODE) has an orbit corresponding to a traveling wave solution of equation (TT). Our primary tool is the Conley Index, as discussed in [26]. We use standard methods [3, 24], but the particular nonlinear structure of (TTODE) requires new a priori bounds and estimates. We rely on the observation that (TTODE) can be rewritten as

$$r(\phi) = -(\arctan(\phi''))', \quad (5.1)$$

when $g(s) = \frac{1}{1+s^2}$. The analysis consequently depends very much on this particular choice of g .

In Section 5.3, we present phase plane illustrations that contrast solutions of (TTODE) to those of (YKODE) and (PMODE). We conclude our discussion of the Tumblin-Turk equations with numerical simulations of equation (TT).

5.1. Lyapunov function for (TTODE). We seek a Lyapunov function, $\mathcal{L}_2(\xi)$, for (TTODE). Let $\mathcal{R}(s)$ denote a primitive of $r(s)$. Multiplying equation (5.1) by ϕ' and integrating produces

$$\mathcal{R}(\phi) = -\arctan(\phi'')\phi' + \int^{\xi} \arctan(\phi''(s))\phi''(s)ds.$$

Since $\arctan(s)s \geq 0$ for all s , we easily check that

$$\mathcal{L}_2(\xi) = \mathcal{R}(\phi(\xi)) + \arctan(\phi''(\xi))\phi'(\xi) \quad (5.2)$$

satisfies

$$\frac{d}{d\xi}\mathcal{L}_2(\xi) = \arctan(\phi''(\xi))\phi''(\xi) \geq 0. \quad (5.3)$$

As was the case for \mathcal{L}_1 , $\mathcal{L}_2(\xi) = \mathcal{R}(\phi(\xi))$ at zeros of ϕ' and ϕ'' . This establishes the entropy condition $\gamma > 0$ and the following lemma.

LEMMA 5.1. *Let $\bar{\phi}$ and $\underline{\phi}$ be defined by (4.5). Any bounded smooth solution ϕ of (TTODE) must satisfy*

$$\underline{\phi} \leq \phi(\xi) \leq \bar{\phi} \quad (5.4)$$

for all $\xi \in \mathbb{R}$.

Proof. The proof follows the same argument as that of Lemma 4.1. \square

5.2. System of ODEs for (TTODE). We rewrite (TTODE) as a system of three ODEs:

$$\phi' = v, \quad v' = \tan(w), \quad w' = -r(\phi). \quad (5.5)$$

System (5.5) has two equilibrium points, $L = (\gamma, 0, 0)$ and $R = (-\gamma, 0, 0)$. We use Conley index theory to prove the existence of a heteroclinic orbit connecting L to R . To do this, we first find uniform bounds for all bounded solutions, (ϕ, v, w) of (5.5). Lemma 5.1 provides such a bound for ϕ . It is particularly important to find a bound C such that $|w| \leq C < \frac{\pi}{2}$. To do so, we first examine $v' = \phi''$.

LEMMA 5.2. *Any bounded smooth solution ϕ of equation (TTODE) satisfies*

$$\int_{-\infty}^{\infty} \arctan(\phi''(s))\phi''(s)ds \leq \mathcal{R}(-\gamma) - \mathcal{R}(\gamma) = \frac{2}{3}\gamma^3. \quad (5.6)$$

Proof. We follow an argument used in the proof of Theorem 4.8 in [4]. Let ϕ be a bounded solution of (TTODE). Bound (5.6) is obvious if either $\phi(\xi) = \gamma$ or $\phi(\xi) = -\gamma$ for all ξ . Since $L = (\gamma, 0, 0)$ and $R = (-\gamma, 0, 0)$ are the only equilibrium points of (TTODE), we now assume that ϕ is nonconstant. We first examine the behavior of $\phi(\xi)$ as $\xi \rightarrow \infty$. There are two cases to consider, depending on the set of extrema of ϕ .

Case 1. Suppose there exists a ξ_M such that ϕ has no extrema for $\xi > \xi_M$. Then ϕ approaches an equilibrium point as $\xi \rightarrow \infty$. Since L is increasing, $\phi \rightarrow -\gamma$ as $\xi \rightarrow \infty$, otherwise all extrema of ϕ would be less than $\underline{\phi}$, and ϕ would grow without bound as $\xi \rightarrow -\infty$. We therefore have

$$\int_0^{\infty} \arctan(\phi''(s))\phi''(s)ds = \mathcal{R}(-\gamma) - \mathcal{R}(\phi(0)).$$

Case 2. Now assume that there is no such ξ_M . Since ϕ solves (TTODE), it is analytic (see e.g. [27]), and must have a countable set of extrema with no limit point. Suppose the extrema occur at ξ_i with $\xi_i > 0$ and $\xi_i < \xi_{i+1}$. The Lyapunov function implies that $\mathcal{R}(\xi_i)$ is a bounded increasing sequence, and we therefore have $\mathcal{R}(\xi) \rightarrow \mathcal{R}_+$, for some $\mathcal{R}_+ \leq \mathcal{R}(-\gamma)$. For each ξ_i ,

$$\int_0^{\xi_i} \arctan(\phi''(s))\phi''(s)ds = \mathcal{R}(\phi(\xi_i)) - \mathcal{R}(\phi(0)) \leq \mathcal{R}(-\gamma) - \mathcal{R}(\phi(0)).$$

The monotone convergence theorem gives us

$$\int_0^{\infty} \arctan(\phi''(s))\phi''(s)ds = \mathcal{R}_+ - \mathcal{R}(\phi(0)) \leq \mathcal{R}(-\gamma) - \mathcal{R}(\phi(0)). \quad (5.7)$$

Similar arguments show

$$\int_{-\infty}^0 \arctan(\phi''(s))\phi''(s)ds \leq \mathcal{R}(\phi(0)) - \mathcal{R}(\gamma). \quad (5.8)$$

Combining (5.7) and (5.8) completes the proof. \square

We interpret Lemma 5.2 to mean that $\phi'' = v'$ is *almost* L^1 , since $\arctan(s)s$ is linear in s for large s . Specifically, for any $\epsilon > 0$, we define $S = \{s : |\phi''(s)| > \epsilon\}$, and discover

$$\begin{aligned} \int_S |\phi''(s)|ds &\leq \frac{1}{\arctan \epsilon} \int_S |\arctan(\phi''(s))\phi''(s)|ds \\ &\leq \frac{1}{\arctan \epsilon} \int_{-\infty}^{\infty} \arctan(\phi''(s))\phi''(s)ds \leq \frac{2}{3 \arctan \epsilon} \gamma^3. \end{aligned} \quad (5.9)$$

We now show that w is bounded away from $\pm \frac{\pi}{2}$, the asymptotes of $\tan w$.

LEMMA 5.3. *Let (ϕ, v, w) be any bounded solution of system (5.5). There exists a positive $C_w < \frac{\pi}{2}$ such that $|w| \leq C_w$ for all $\xi \in \mathbb{R}$.*

Proof. Since ϕ is uniformly bounded, $|-r(\phi)| \leq M$ for some M , which by (5.5) implies a uniform Lipschitz bound for w ,

$$w(\xi_0 - h) \geq w(\xi_0) - Mh, \text{ for all } \xi_0 \text{ and all } h > 0. \quad (5.10)$$

We use (5.9) with the uniform Lipschitz continuity of w to derive a point-wise bound on w . We focus on bounding w away from $w = +\frac{\pi}{2}$. To make use of (5.9), we must find an interval on which w is bounded away from zero. Pick ξ_0 with $\frac{\pi}{4} < w(\xi_0) < \frac{\pi}{2}$. If no such ξ_0 exists, then $w(\xi) \leq \frac{\pi}{4}$. Choose $\delta > 0$ so

$$\frac{\pi}{4} > w(\xi_0) - M\delta \geq \frac{\pi}{6}, \quad (5.11)$$

also implying by (5.10) that $w(\xi) \geq \frac{\pi}{6}$ for all $\xi \in [\xi_0 - \delta, \xi_0]$. Let

$$S = \{\xi : \phi''(\xi) \geq \frac{\sqrt{3}}{3} = \tan \frac{\pi}{6}\}.$$

Then Lemma 5.2 ensures

$$\int_S |v'| = \int_S |\phi''| \leq \frac{6}{\pi} (\mathcal{R}(-\gamma) - \mathcal{R}(\gamma)) = \frac{4}{\pi} \gamma^3. \quad (5.12)$$

Now using (5.10) and (5.11), we calculate

$$\begin{aligned} \int_S |v'(s)| ds &\geq \int_{\xi_0 - \delta}^{\xi_0} |v'(s)| ds \\ &= \int_{\xi_0 - \delta}^{\xi_0} |\tan(w(s))| ds \\ &\geq \int_{\xi_0 - \delta}^{\xi_0} \tan(w(\xi_0) - M(\xi_0 - s)) ds \\ &= \frac{1}{M} \log \left| \frac{\cos(w(\xi_0) - M\delta)}{\cos(w(\xi_0))} \right| \\ &\geq \frac{1}{M} \log \left| \frac{\cos \frac{\pi}{4}}{\cos(w(\xi_0))} \right|. \end{aligned}$$

Combining this with (5.12), we see

$$\frac{1}{M} \log \left| \frac{\sqrt{2}}{2 \cos(w(\xi_0))} \right| \leq \frac{4}{\pi} \gamma^3, \quad (5.13)$$

so

$$\cos(w(\xi_0)) \geq \frac{\sqrt{2}}{2} e^{-M(\frac{4}{\pi} \gamma^3)} > 0, \quad (5.14)$$

and

$$w(\xi_0) \leq \arccos\left(\frac{\sqrt{2}}{2} e^{-M(\frac{4}{\pi} \gamma^3)}\right) < \frac{\pi}{2}. \quad (5.15)$$

The same argument with slight adjustments shows that

$$w(\xi_0) \geq -\arccos\left(\frac{\sqrt{2}}{2}e^{-M(\frac{4}{\pi}\gamma^3)}\right) > -\frac{\pi}{2}.$$

□

COROLLARY 5.4. *There exists a $C_v > 0$ satisfying $|v| \leq C_v$.*

Proof. Since w is bounded in an interval strictly contained within $(-\frac{\pi}{2}, \frac{\pi}{2})$, we have a bound on $\phi'' = \tan w$. We use Lemma 4.4 to bound $v = \phi'$. □

THEOREM 2. *Given any $\gamma > 0$, there exists a solution ϕ of (TTODE) such that $\phi(\xi) \rightarrow \gamma$ as $\xi \rightarrow -\infty$, and $\phi(\xi) \rightarrow -\gamma$ as $\xi \rightarrow \infty$.*

Proof. Our proof centers on the Conley Index. We refer our reader to [26], which contains an excellent description of Conley Index theory. Let C_v and C_w be given by Lemmas 5.4 and 5.3. Define the set

$$N = \left\{ (\phi, v, w) : \begin{array}{l} \underline{\phi} \leq \phi \leq \bar{\phi} \\ |v| \leq C_v \\ |w| \leq C_w \end{array} \right\}. \quad (5.16)$$

N is an isolating neighborhood, as all bounded trajectories are strictly contained within the interior of N . As explained in Theorem 22.18 of [26], N contains an isolating block, B . Isolating blocks of (TTODE) are special isolating sets whose boundary points immediately leave the set in positive or negative time under the flow defined by (TTODE). The Conley Index is the homotopic equivalence class of the quotient space B/b^+ , where b^+ is the set of all points on ∂B that leave B in positive time. Let $\beta \in \mathbb{R}$, and define the continuous deformation of (TTODE),

$$r(\phi) + \beta = -(g(\phi'')\phi'''). \quad (5.17)$$

Let $\beta_0 = \frac{\pi}{2}$. For $\beta < \beta_0$, B contains two equilibrium points, and B can also be chosen large enough so that it is an isolating block of (5.17) for all $\beta < \beta_0$, as uniform bounds can be found on the set of all bounded trajectories as was done above for the case $\beta = 0$.

When $\beta = \beta_0$, the only bounded trajectory of (5.17) is the constant function $\phi = 0$, so B remains an isolating block. Choosing $\beta > \beta_0$ produces a differential equation with no equilibrium points. B remains an isolating block of the flow, and contains no isolated invariant set (other than the null set). It follows that the homotopic equivalence class of B/b^+ is that of the null set, implying the existence of an orbit of (TTODE) connecting L and R (see Theorem 22.33 in [26]). The Lyapunov function ensures that the trajectory flows from L to R . □

5.3. The (TTODE) phase space. As suggested by our analysis of both equations, the phase plane geometry of (TTODE) is remarkably different from that of equation (YKODE). Using the method discussed in Section 4.4, we visualize the phase space by considering the cross-section $u = 0$, denoted by Σ_0 . Any intersection of $W^u(L)$ with $W^s(R)$ is visible on Σ_0 , where it must occur on the line $w = 0$. We draw $W^u(L)$ by computing trajectories with initial conditions near L , and marking their intersections with Σ_0 . $W^s(R)$ is drawn similarly, but by numerically integrating (TTODE) backward in time.

Smooth curves in the phase space must lie between the two planes $w = \pm\frac{\pi}{2}$, since $v = \tan w$. Figures 5.1 and 5.2 show the intersections of $W^s(R)$ and $W^u(L)$ with Σ_0 for various values of γ . Since $W^s(R)$ and $W^u(L)$ do not have boundaries caused by

singularities of (TTODE), both manifolds stretch from $w = -\frac{\pi}{2}$ to $w = \frac{\pi}{2}$, even for large γ . This allows an intersection at $w = 0$ for all $\gamma > 0$; increasing γ only shifts the manifolds in the $-v = -\phi'$ direction. This is remarkably different from the You-Kaveh ODE (YKODE), for which $W^s(R)$ and $W^u(L)$ have boundaries that allow the manifolds to shift away from each other when γ is increased.

5.4. Traveling wave solutions of equation (TT). Figure 5.3 shows traveling wave solutions of equation (TT) for a series of γ -values. Each traveling wave was produced by finding the intersection of $W^u(L)$ with $W^s(R)$ in the phase space of (TTODE). As the jump height from u_L to u_R increases, so does the traveling wave's slope near the jump. Although the ODE solutions are smooth, the jump transition can be so severe that when viewed at large length scales, the solution appears to have a shock. This is demonstrated when $\gamma = 7$, as shown in Figure 5.3.

Numerical examples suggest that the heteroclinic orbits of (TTODE) are stable traveling wave solutions of equation (TT). To numerically integrate equation (TT), we use the change of variables $w = \arctan u_{xx}$, and solve the nonlinear system

$$\begin{aligned} u_t + uu_x &= w_{xx} \\ \tan w &= -u_{xx} \end{aligned} \tag{5.18}$$

using a fully implicit scheme. The change of variables $w = \arctan u_{xx}$ is used to ensure that u_{xx} remains bounded. See [5] for a discussion on numerically implementing the fourth order diffusion.

Figure 5.4 shows the behavior of u , given an initial condition near the traveling wave profile. The computations suggest that the traveling wave is a stable solution of the PDE.

Intersections of $W^s(R_\gamma)$ and $W^u(L_\gamma)$ With Σ_0
 $\gamma = 1.0$ and $\gamma = 2.0$

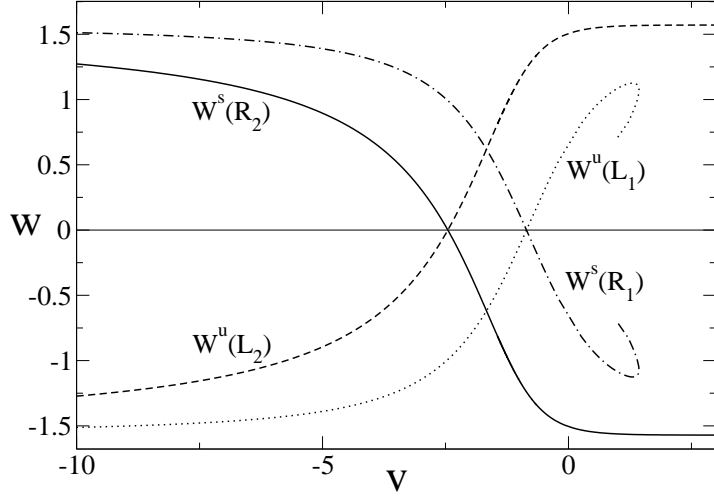


FIG. 5.1. Changes of the manifolds for (TTODE) with increasing γ . The intersections of $W^u(L)$ and $W^s(R)$ with Σ_0 are shown for $\gamma = 1.0$ and $\gamma = 2.0$.

Intersections of $W^s(R_\gamma)$ and $W^u(L_\gamma)$ With Σ_0
 $\gamma = 2.0, 5.0$ and 8.0

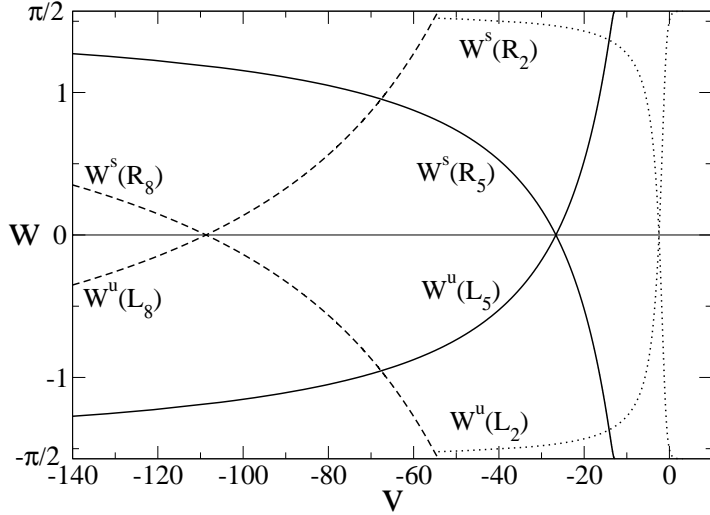


FIG. 5.2. Changes of the manifolds for (TTODE) with increasing γ . The intersections of $W^u(L)$ and $W^s(R)$ with Σ_0 are shown for $\gamma = 2.0, 5.0,$ and 8.0 . Each manifold's structure persists while increasing γ .

Tumblin-Turk Traveling Waves

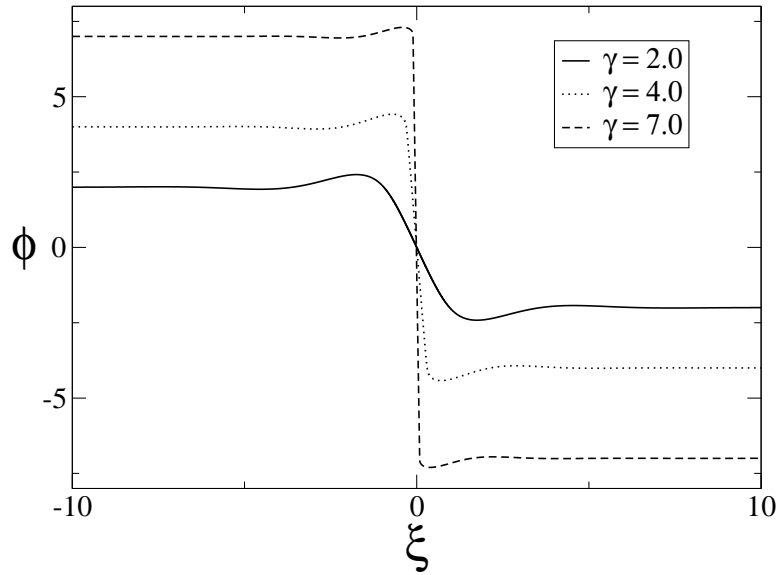


FIG. 5.3. **Heteroclinic orbits of equation (TTODE).** *At this length scale, the traveling wave solution for $\gamma = 7$ appears to have a shock.*

Tumblin-Turk with Advection $\gamma = 7.0$

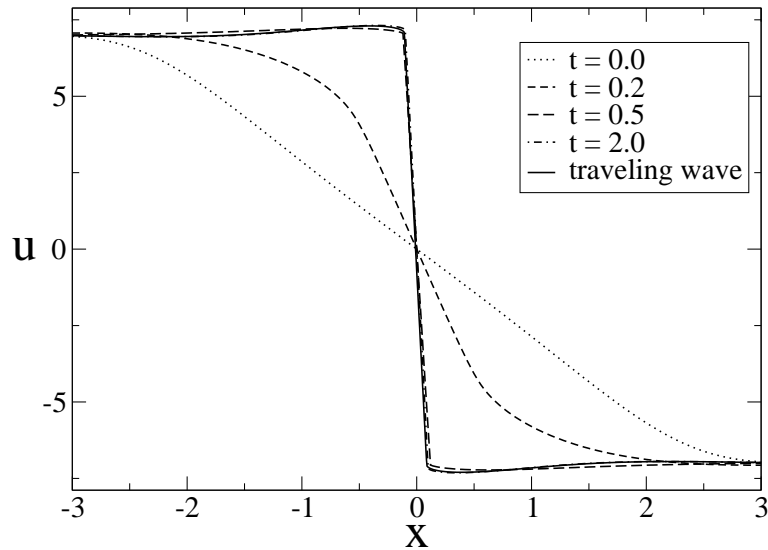


FIG. 5.4. **Numerically integrated solution of equation (TT) for $\gamma = 7.0$.**

6. Conclusions. We have considered traveling wave solutions of the advection diffusion equations

$$u_t + \left(\frac{1}{2}u^2\right)_x = -(g(u_{xx})u_{xx})_{xx} \quad (YK)$$

and

$$u_t + \left(\frac{1}{2}u^2\right)_x = -(g(u_{xx})u_{xxx})_x, \quad (TT)$$

with $g(s) = \frac{1}{1+s^2}$, in order to cleanly illustrate the features of higher order nonlinear diffusion equations recently proposed for use in image processing.

The advection term uu_x in (YK) and (TT) serves two roles. First it allows for traveling wave solutions that approximate shocks, which in images correspond to edges. By converting the problem to one of traveling waves, we reduce a fourth order PDE to a third order ordinary differential equation for which we are able to prove rigorous results and perform clear phase space computations. Second, advective PDEs combining similar diffusion terms are being used for such processes as image inpainting [1, 2]. Thus these kind of equations are interesting for image processing in their own right.

We discover a fundamental difference between solutions of (YK) and (TT). Smooth traveling waves solutions of (YK) do not exist for sufficiently large jump height, whereas solutions of (TT) exist for all jumps. This suggests that the dynamics of the full PDE (YK) is quite different from that of (TT). In a separate paper, we prove that in one dimension, the PDE (TT) without advection has globally smooth solutions, given smooth initial data. The study in this paper would lead us to conjecture that (YK) without advection does have finite time singularities in u_{xx} , just as the classical Perona-Malik equation has finite time singularities in the slope.

Although the PDE numerics suggest that the smooth traveling waves are stable, a rigorous proof of this is still forthcoming. Osher and Ralston addressed the same problem in [22], where they proved stability of traveling waves of the convective porous media equation. More recently, the authors of [6] used Evans function techniques to prove stability of thin film traveling waves.

REFERENCES

- [1] Marcelo Bertalmio, Andrea Bertozzi, and Guillermo Sapiro. Navier-Stokes, fluid-dynamics and image and video inpainting. In *IEEE CVPR 2001, Hawaii*, volume I, December 2001.
- [2] Marcelo Bertalmio, Guillermo Sapiro, Vincent Caselles, and Coloma Ballester. Image inpainting. In *SIGGRAPH*, pages 417 – 424, 2000.
- [3] A. L. Bertozzi, A. Münch, and M. Shearer. Undercompressive shocks in thin film flows. *Phys. D*, 134(4):431–464, 1999.
- [4] A. L. Bertozzi and M. Shearer. Existence of undercompressive traveling waves in thin film equations. *SIAM J. Math. Anal.*, 32(1):194–213 (electronic), 2000.
- [5] Andrea L. Bertozzi and John B. Greer. Low curvature image simplifiers: global regularity of smooth solutions and Laplacian limiting schemes, 2003. preprint.
- [6] Andrea L. Bertozzi, Andreas Münch, Michael Shearer, and Kevin Zumbrun. Stability of compressive and undercompressive thin film travelling waves. *European J. Appl. Math.*, 12(3):253–291, 2001.
- [7] R. Buckingham, M. Shearer, and A. L. Bertozzi. Thin film traveling waves and the navier slip condition. *SIAM J. Appl. Math.*, accepted 2002.
- [8] Francine Catte, Pierre-Louis Lions, Jean-Michel Morel, and Tomez Coll. Image selective smoothing and edge detection by nonlinear diffusion. *SIAM. J. Num. Anal.*, 29(1):182–193, 1992.

- [9] A. Chambolle and P.-L. Lions. Image recovery via total variation minimization and related problems. *Numer. Math.*, 76:167–188, 1997.
- [10] T. Chan, A. Marquina, and P. Mulet. High-order total variation-based image restoration. *SIAM J. Sci. Comp.*, 22(2):503–516, 2000.
- [11] Selim Esedoglu. *An analysis of the Perona-Malik Scheme*. PhD thesis, Courant Institute of Mathematical Sciences, NYU, July 2000.
- [12] Selim Esedoglu. An analysis of the Perona-Malik scheme. *Comm. Pure Appl. Math.*, 54(12):1442–1487, 2001.
- [13] Jonathan Goodman, Alexander Kurganov, and Philip Rosenau. Breakdown in Burgers-type equations with saturating dissipation fluxes. *Nonlinearity*, 12(2):247–268, 1999.
- [14] J. B. Greer and A. L. Bertozzi. H^1 solutions of a class of fourth order nonlinear equations for image processing. *Discrete and continuous dynamical systems*, 2003. to appear.
- [15] Satyanad Kichenassamy. The Perona-Malik paradox. *SIAM J. Appl. Math.*, 57(5):1328–1342, 1997.
- [16] A. Kurganov and P. Rosenau. Effects of a saturating dissipation in Burgers-type equations. *Comm. Pure Appl. Math.*, 50(8):753–771, 1997.
- [17] Alexander Kurganov, Doron Levy, and Philip Rosenau. On Burgers-type equations with non-monotonic dissipative fluxes. *Comm. Pure Appl. Math.*, 51(5):443–473, 1998.
- [18] Peter D. Lax. *Hyperbolic systems of conservation laws and the mathematical theory of shock waves*. Society for Industrial and Applied Mathematics, Philadelphia, Pa., 1973. Conference Board of the Mathematical Sciences Regional Conference Series in Applied Mathematics, No. 11.
- [19] Marius Lysaker, Arvid Lundervold, and Xue-Cheng Tai. Noise removal using fourth-order partial differential equations with applications to medical magnetic resonance images in space and time, 2002. UCLA CAM preprint 02-44.
- [20] Marius Lysaker, Stanley Osher, and Xue-Cheng Tai. Noise removal using smoothed normals and surface fitting, 2003. UCLA CAM preprint 03-03.
- [21] D. Mumford and J. Shah. Optimal approximations by piecewise smooth functions and associated variational problems. *Comm. Pur. Appl. Math.*, 42:577–685, 1989.
- [22] Stanley Osher and James Ralston. L^1 stability of travelling waves with applications to convective porous media flow. *Comm. Pure Appl. Math.*, 35(6):737–749, 1982.
- [23] P. Perona and J. Malik. Scale-space and edge detection using anisotropic diffusion. *IEEE Trans. Pattern Anal. Machine Intell.*, 12:629–639, 1990.
- [24] Michael Renardy. A singularly perturbed problem related to surfactant spreading on thin films. *Nonlinear Anal.*, 27(3):287–296, 1996.
- [25] L. Rudin, S. Osher, and E. Fatemi. Nonlinear total variation based noise removal algorithms. *Physica D*, 60:259–268, 1992.
- [26] Joel Smoller. *Shock waves and reaction-diffusion equations*, volume 258 of *Grundlehren der Mathematischen Wissenschaften [Fundamental Principles of Mathematical Sciences]*. Springer-Verlag, New York, second edition, 1994.
- [27] Michael E. Taylor. *Partial differential equations. I*. Springer-Verlag, New York, 1996. Basic theory.
- [28] Jack Tumblin and Greg Turk. LCIS: A boundary hierarchy for detail-preserving contrast reduction. In *Proceedings of the SIGGRAPH 1999 annual conference on Computer graphics, August 8-13, 1999, Los Angeles, CA USA*, pages 83–90, 1999. <http://www.acm.org/pubs/citations/proceedings/graph/311535/p83-tumblin/>.
- [29] Guo W. Wei. Generalized Perona-Malik equation for image processing. *IEEE Signal Processing Letters*, 6(7):165–167, July 1999.
- [30] Joachim Weickert, Bart M. ter Haar Romeny, and Max A. Viergever. Efficient and reliable schemes for nonlinear diffusion filtering. *IEEE Transactions on image processing*, 7(3):398–410, March 1998.
- [31] R. Whitaker and S. Pizer. A multi-scale approach to nonuniform diffusion. *CVGIP:Image Understanding*, 57(1):99–110, 1993.
- [32] Yu-Li You and M. Kaveh. Fourth-order partial differential equations for noise removal. *IEEE Trans. Image Process.*, 9(10):1723–1730, 2000.